Impacts of environmental levels of hydrogen peroxide and oxyanions on the redox activity of MnO2 particles

Daqing Jia, Qinzhi Li, Tao Luo, Olivier Monfort, Gilles Mailhot, Marcello Brigante, Khalil Hanna

Impacts of environmental levels of hydrogen peroxide and oxyanions on the redox activity of MnO_2 particles

Daqing Jia[a], Qinzhi Li[b], Tao Luo[b], Olivier Monfort[d], Gilles Mailhot[a], Marcello Brigante[a], Khalil Hanna[b,c*]

[a] *Université Clermont Auvergne, CNRS, Clermont Auvergne INP, Institut de Chimie de Clermont-Ferrand, F-63000 Clermont-Ferrand, France.*

[b]*Univ. Rennes, École Nationale Supérieure de Chimie de Rennes, CNRS, ISCR UMR 6226, F-35000 Rennes, France*

[c]*Institut Universitaire de France (IUF), MESRI, 1 rue Descartes, 75231 Paris, France.*

[d]*Comenius University in Bratislava, Faculty of Natural Sciences, Department of Inorganic Chemistry, Ilkovicova 6, Mlynska Dolina, 842 15 Bratislava, Slovakia.*

*Corresponding author: +33 2 23 23 80 27, khalil.hanna@ensc-rennes.fr

Abstract

Despite the widespread presence of hydrogen peroxide in surface water and groundwater systems, little is known about the impact of environmental levels of H_2O_2 on the redox activity of minerals. Here we demonstrate that environmental concentrations of H_2O_2 can alter the reactivity of birnessite-type manganese oxide, an earth-abundant functional material, and decrease its oxidative activity in natural systems across a wide range of pH values (4-8). The H_2O_2-induced reductive dissolution generates Mn(II) that will re-bind to MnO_2 surfaces, thereby affecting the surface charge of MnO_2. Competition of Bisphenol A (BPA), used as a target compound here, and Mn(II) to interact with reactive surface sites may cause suppression of the oxidative ability of MnO_2. This suppressive effect becomes more effective in presence of oxyanions such as phosphate or silicate at concentrations comparable to those encountered in natural waters. Unlike nitrate, adsorption of phosphate or silicate onto birnessite increased in presence of Mn(II) added or generated through H_2O_2-induced reduction of MnO_2. This suggests that naturally occurring anions and H_2O_2 may have synergetic effects on the reactivity of birnessite-type manganese oxide at a range of environmentally relevant H_2O_2 amounts. As layered structure manganese oxides play a key role in the global carbon cycle as well as pollutant dynamics, the impact of environmental levels of hydrogen peroxide (H_2O_2/MnO_2 molar ratio ≤ 0.3) should be considered in environmental fate and transport models.

Keywords: birnessite; redox; hydrogen peroxide; oxyanion.

Table of contents

H_2O_2/MnO_2 molar ratio as low as 0.03 can affect the redox activity of MnO_2 particles and their reactivity in natural systems.

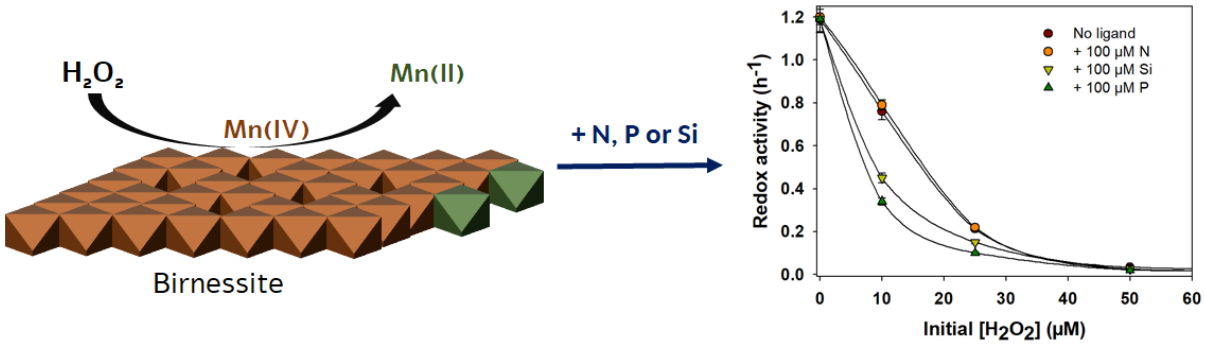

Introduction

Layered structure manganese oxides (*e.g.* birnessite) are ubiquitous in a wide range of aquatic and terrestrial environments.[1] The presence of exchangeable hydrated cations within the interlayers combined with a high content of vacancy sites and variable oxidation states of manganese make them powerful sorbents and oxidants.[2,3] As a result, birnessite-type manganese oxides play a significant role in controlling the cycles of several key nutrients as well as the fate and mobility of inorganic and organic contaminants.[4-9] Acid birnessite has been widely investigated because it is structurally similar to biogenic "natural" manganese oxides.[10-13] The birnessite reactivity is mainly affected by solution pH, surface properties and composition of MnO_2 and structural characteristics of redox-active contaminants.[4-6,12] It can also be influenced by the presence of naturally occurring compounds, *e.g.* cations, anions, natural organic matter and other redox-active compounds. Among the latter, hydrogen peroxide (H_2O_2) has an ambivalent redox activity and is commonly found in aquatic environments at concentration ranging from nM to µM.[14-26]

In environmental systems, photodependent reactions mediated by natural organic matter and biological-mediated processes dominate H_2O_2 production.[26] Sunlight-induced photochemical reactions mediated by organic ligands and/or biochemical metabolic processes can result in amounts of H_2O_2 up to 20 µM.[14-18] Input from rainwater can reach up to 40 µM [20,21], while hydrogen peroxide production has been often observed in irradiated seawater.[19-21] Light-independent generation of H_2O_2 has been recently reported in river sediments and in groundwater of an alluvial aquifer, which is likely to occur in transitional redox environments where reduced elements react with oxygen.[22,23] For example, natural hydroquinones or hydroquinone moieties ubiquitously present in reduced organic matter can donate electrons to O_2 to generate H_2O_2.[24,25] H_2O_2 production through microbial mechanism has also been shown to enhance iodide oxidation and organo-iodine formation in soils and sediments.[27]All these

studies suggested that H_2O_2 can be formed not only in oceanic and atmospheric systems but also in the subsurface environment. Finally, higher concentrations (up to 1 mM) have been reported in nuclear waste repository scenarios when ionizing radiation of groundwater adjacent to spent nuclear fuel result in H_2O_2 production.[28]

Despite the catalyzed decomposition of hydrogen peroxide by MnO_2 has been well investigated [29-31], knowledge is very limited on the effect of H_2O_2 on the reactivity of birnessite at environmental levels of H_2O_2. In engineering applications, metal oxides such as MnO_2 are generally investigated for catalytic decomposition of H_2O_2 and then formation of reactive transient species using very high concentrations of hydrogen peroxide (H_2O_2) ($\geq$ 0.5 mM). [29-31] While these remediation studies aimed to eliminate pollution in contaminated systems, they overlooked the influence of H_2O_2 on the electron transfer heterogeneous reaction and then the oxidative activity of birnessite. In addition, little is known about the influence of H_2O_2 on the birnessite composition and interactions of redox products (*e.g.* Mn(II)) with MnO_2 surfaces.

In this study, we examine how H_2O_2 affects the reactivity of birnessite under environmentally relevant conditions. To monitor H_2O_2-induced changes in birnessite reactivity, we used Bisphenol A (BPA) as a model compound because it has a strong reactivity with the birnessite (δ-MnO_2), with a well-documented underlying redox mechanism.[32-35] Acid birnessite, a well-established laboratory synthesized analog of layered birnessite mineral, was chosen as a representative manganese dioxide mineral. The removal kinetics of BPA have been assessed in presence of variable amounts of H_2O_2 under a wide range of pH (4, 6.5 and 8) under aerobic and anaerobic conditions. Alteration of birnessite structure and composition was monitored using XRD and titration experiments under different conditions (H_2O_2/MnO_2 molar ratio, dissolved Mn(II) amount and pH value). To check whether the impact of H_2O_2 can persist in natural waters, changes in birnessite reactivity were investigated in presence of commonly found anionic ligands such as phosphate, nitrate and silicate. We notably demonstrated that at

H_2O_2 concentrations as low as 10 μM or with H_2O_2/MnO_2 molar ratio as low as 0.03, the reactivity of acid birnessite can be affected, which could alter biogeochemical cycles as well as pollutant dynamics.

2. Materials and Methods

2.1. Chemicals

$KMnO_4$, HCl, NaCl, NaOH, HEPES, $H_2C_2O_4$, H_2SO_4,hydroxylamine hydrochloride, H_2O_2, BPA, HNO_3, terephthalic acid, 2-hydroxyterephthalic acid, Na_2SiO_3, $NaNO_3$, NaH_2PO_4 and $MnCl_2$were purchased from Sigma-Aldrich and were all AR grade. All chemicals were used as received without further purification. All solutions were prepared in ultrapure water obtained from a water purification system (Millipore, resistivity 18.2 MΩ cm).

2.2. Synthesis and characterization of acid birnessite

Acid birnessite was prepared following the procedure of McKenzie[36], and Mn(III)-rich MnO_2 was synthesized according to previous published methods.[37,38] More details are provided in the Supporting Information (SI). The solid was characterized using X-ray powder diffraction (XRD) using the Bruker AXS D8 Advance diffractometer (θ-2θ Bragg-Brentano geometry) using monochromatized CuKα1 (1.54Å) radiation over the range of 10º-100º 2θ at a step size of 0.02º. X-ray diffraction (XRD) confirmed that the only product of the synthesis was poorly-crystalline hexagonal birnessite. The Brunauer−Emmett−Teller (BET) specific surface area of the synthetic birnessite measured by multipoint N_2 adsorption was 60 ± 2.5 (SD) $m^2\ g^{-1}$. The Average Oxidation State (AOS= 3.98 (±0.02)) of synthetic birnessite and (AOS= 3.65 (±0.02)) of Mn(III)-rich MnO_2 were measured using the oxalic acid-permanganate back-titration method (more details are provided in SI). Scanning Electron Microscope (SEM; JEOL JSM-7100F) and

High-resolution Transmission Electron Microscope (HRTEM; JEOL 2100 LaB_6) images showed a nanoflower-shaped birnessite consisting of nanoflakes aggregations (see Figure S1).

2.3. Kinetics experiments and analyses

Reactivity changes assessment were investigated as following: 100 mL aqueous suspension of acid birnessite (AB) corresponding to an initial concentration of 345 μM was first prepared and then an appropriate amount of stock solutions of H_2O_2, BPA, and/or Mn(II) were added to start the reaction at room temperature. Since the involved reactions can consume protons (see below), the pH was adjusted to the desired value and then kept constant throughout the reaction using a pH meter (Cyberscan 510, Thermo Scientific) by adding 0.1 M NaOH or HCl. The suspension was stirred with a speed of 350 rpm. 1 mL of aqueous sample was withdrawn at different time interval, filtered through 0.22 μm PTFE filter, and then analyzed. The same batch experiments were carried out in the presence of silicate or phosphate to evaluate the combined effects of anions and H_2O_2 on BPA oxidation.

Potential generation of hydroxyl radical was monitored through the fluorescence emission spectrum of 2-hydroxyterephthalic acid (λ_{ex} 320 nm, λ_{em} 425 nm) using a spectrofluorometer (Shimadzu RF-5301PC) (more information is given in the SI).

The BPA concentration was determined by a high-performance liquid chromatography system (HPLC, Waters Alliance) equipped with a diode array detector (DAD). Chromatographic separation was performed using a Nucleodur 100-5 C18 column (150 × 4.6 mm, 5 μm of particle size, Macherey Nagel). The detection wavelength of BPA was set at 277 nm and the column temperature was kept at 30 °C. Methanol and water were mixed as the mobile phase under a gradient eluent mode, and the percentage of methanol changed with time was as follows: from 0 to 7 min was increased from 70 to 90% and kept constant up to 9 min. The flow rate was set at 0.8 mL min^{-1}. The byproducts of BPA oxidation were identified using Ultraperformance Liquid Chromatography-tandem Mass Spectrometry (UPLC-MS/MS)

system. An electrospray interface was used for the MS measurements in positive ionisation mode and full scan acquisition.

H_2O_2 concentration was determined using a spectrofluorometric detection as described in our previous work.[39] Briefly, samples containing H_2O_2 were mixed with 4-hydroxyphenylacetic acid to form the stable 4-hydroxyphenyl acetic acid dimer in the presence of peroxidase (POD, Sigma-Aldrich). The 4-hydroxyphenylacetic acid dimer was quantified using a Cary Eclipse fluorescence spectrophotometer. The excitation wavelength was set at 320 nm and emission wavelength maximum was determined at 420 nm. Concentration was calculated using calibration curve obtained using different concentrations of H_2O_2.[40]

Dissolved Mn(II) concentration in aqueous solution was determined by Atomic Absorption Spectroscopy (AAS, PerkinElmer). All the samples were first filtered using a PTFE 0.22 μm filter and then mixed with 2% nitric acid (HNO_3, 65%, Sigma- Aldrich) prior for analyses. Dissolved Mn(II) standard solution for AAS (TraceCERT®, 1000 mg L^{-1} Mn(II) in 2% nitric acid, Sigma-Aldrich) was used for the calibration curve. The detection wavelength was set at 279 nm and the AAS detection limit lied at 0.02 μM. Mn(II) removal was calculated as the difference between the initial and final Mn(II) solution concentrations.

The impact of anions on reactivity changes was investigated as mentioned above, but with addition of the chosen anion with BPA or Mn(II) to the AB suspension. Silicate concentration was determined by the molybdenum-blue colorimetric method[41] while phosphate and nitrate concentrations by ion chromatography.[42] XRD was performed to determine the possible transformation of solids upon Mn(II) sorption.

Since Mn(II) oxidation by molecular oxygen may take place, particularly at alkaline pH values, we compared the removal kinetics under aerobic (open atmosphere) *vs* anaerobic conditions (glove box N_2:H_2 98:2). Prior for anoxic experiments, all solutions were sparged with nitrogen to remove oxygen. These preliminary tests showed that there is no effect of oxic

conditions on the BPA removal in presence of H_2O_2 or Mn(II). Great attention has also been paid to the pH adjustment in all experiments, since the involved reactions are sensitive to pH value (see below). All experiments were conducted in triplicates and the standard deviation was calculated for all experimental series, and given in the caption of each figure.

3. Results and Discussion

3.1 Effect of H_2O_2 on the oxidative ability of birnessite

BPA removal was monitored in the presence of acid birnessite (AB) at different H_2O_2 concentrations at pH 6.5 (Fig. 1). In the absence of H_2O_2, almost complete removal of BPA was observed after 24h of reaction time. Mass balance showed that the oxidation reaction was mainly involved in the removal of BPA in presence of MnO_2, while adsorption was very low under our experimental conditions (*i.e.* less than 5% of initial BPA), which is consistent with previous investigations.[6,32,33] Indeed, BPA containing two hydroxyphenyl functionalities is known to weakly interact with mineral surfaces, resulting in lower adsorption affinity to metal-oxides.[32] As previously reported, [6,33,43] binding to birnessite is followed by an electron transfer process resulting in the concomitant oxidation of sorbed compound and reduction of surface-bound Mn(IV) to yield Mn(III) that can be further reduced to give Mn(II).

$$Mn^{IV}O_2 + BPA + 4\ H^+ \rightarrow Mn^{II} + BPA_{ox} + 2\ H_2O \qquad \text{(Eq.1)}$$

Electron exchange of BPA with MnO_2 form a radical, followed by a series of reactions including radical coupling, fragmentation, substitution and elimination to form multiple byproducts. [6,32,33] LC/MS analysis identified one predominant species of mass-to-charge ratio of m/z = 135 as the most dominant byproduct of BPA over the first reaction time (90 min), which likely corresponds to 4-hydroxycumyl alcohol according to previous investigations. [44]

In the presence of hydrogen peroxide, the oxidative removal of BPA gradually decreased with increasing in H_2O_2 concentration, and completely suppressed at higher dose of H_2O_2 (200

μM equivalent to a H_2O_2/MnO_2 molar ratio ~ 0.6). In these experiments, the H_2O_2 decomposition is relatively fast whatever the investigated pH, since complete decomposition of H_2O_2 was achieved after 15 min of reaction, even for the highest H_2O_2 dose (See Fig. S2 and S3). Monitoring of fluorescence emission spectra of suspensions using a terephthalate as a chemical probe indicated that no hydroxyl radical was generated under the experimental conditions of this study. Additional experiments using 1-propanol (1 mM) or t-butanol (1 mM) as hydroxyl-radical scavengers confirmed that the BPA removal is a no radical-based oxidation process regardless of the presence or absence of H_2O_2.

The suppressive effect of H_2O_2 on the removal rate of BPA was then confirmed at two other pH values (4 and 8). The removal kinetics could not be properly described by simple equations that include classical exponential functions (*e.g.,* first- or second- order model), probably due to the complexity of involved reactions in the investigated system. Instead, we calculated the initial rate constant (k, h^{-1}) by linear regression of ln [BPA] /$[BPA]_o$ versus time over the first stage of reaction (see example in Fig. S4). The initial rate constants for all investigated H_2O_2 amounts exhibited the same order, pH 4 > pH 6.5 > pH 8 (Fig. 2). In the absence of H_2O_2, k was decreased almost 20-fold when pH increased from 4 to 8. This suggests that acidic conditions favored BPA removal, a trend also observed for other organic compounds reacting with MnO_2. [33,34,45] We attribute this to variability in two pH-dependent factors: 1) speciation of BPA that affects binding to MnO_2 surfaces and then oxidation (Fig. S5), and 2) redox-potential of MnO_2 that decreases when the pH increased from 4 to 8. [46] At relatively low pH, favorable electrostatic interactions between neutral BPA molecules and the negatively charged surface of MnO_2 (PZC of MnO_2 is ~ 2.3-2.9) may exist. On the other hand, reductive conversion of MnO_2 into Mn(II) is dependent on the amount of protons, which would result in increase in BPA removal rate when the pH decreases (Eq.1). In the presence of H_2O_2, the removal rate constants of BPA sharply decreased with increasing in H_2O_2 amount whatever the investigated pH value (Fig. 2).

As for BPA, it is previously reported that hydrogen peroxide can also reduce Mn(IV) to Mn(III) and then Mn(II) as follows [47,48] :

$$Mn^{IV}O_2 + H_2O_2 + 2\ H^+ \rightarrow Mn^{II} + O_2 + 2\ H_2O \quad \text{(Eq.2)}$$

To check this possibility under our experimental conditions, the reductive dissolution of MnO_2 in presence of various amounts of H_2O_2 was monitored at three pH values (Fig. 3). In both Eq.1 and Eq.2, protons are directly involved in the oxidation of BPA as well as the reductive dissolution of MnO_2. In the absence of H_2O_2, dissolved Mn(II) was only detected at pH 4, while it was below the detection limit at pH 6.5 or 8. Increasing H_2O_2 concentration from 50 µM to 200 µM enhanced the amount of dissolved Mn(II), at the three investigated pH values. At each pH value, the amount of dissolved Mn(II) increased first, reached a maximum and then decreased. This two-step behavior is consistent with the H_2O_2 decomposition over time, where the complete decomposition of H_2O_2 observed after approximately 15 min of reaction time coincides with the peak observed for dissolved Mn(II) generation (Fig. S3). This behavior also suggests that the production of Mn(II) via H_2O_2-induced reduction of MnO_2 is faster than the Mn(II) adsorption onto birnessite. Once the added H_2O_2 is fully decomposed, the generated dissolved Mn(II) will in turn sorb onto MnO_2 surfaces.

Because higher pH implies more Mn(II) binding[49-51], greater amounts of Mn(II) were observed at low pH values (Fig. 3). When a further addition of H_2O_2 is made after total decomposition of the initial amount (*e.g.* after 15 min at pH 4), the amount of generated Mn(II) increased again and reached almost twice the first measured amount within approximately 15 min. This suggests that the reductive dissolution of MnO_2 by H_2O_2 is a fast process, as compared to the reaction between MnO_2 and BPA.

To check whether Eq.1 and Eq.2 may occur simultaneously during the heterogeneous reactions with MnO_2, we compare the standard potential of involved reactions at the working

pH range. MnO_2 has standard (reduction) potential varying from 0.99 to 0.76 V when the pH rises from 4 to 8 for $MnO_2 + 4\ H^+ + 2\ e^- \rightarrow Mn^{II} + 2\ H_2O$. This value is higher than the standard oxidation potential of O_2/H_2O_2 ($O_2 + 2\ H^+ + 2e^- \rightarrow H_2O_2$ 0.68 V *vs.* NHE) or of BPA which varies between 0.75 V and 0.52 V in the pH range 4-8.[52-54] Since the latter redox couples have comparable oxidation potential, reactions (Eq.1) and (Eq.2) could simultaneously take place. Assuming that these reactions obey pseudo-first order kinetic equation because MnO_2 is considered in excess, the reaction rate depends on the concentration of reactants (*i.e.* H_2O_2 or BPA). When the H_2O_2 amount increases, the reaction 2 should become much faster than the reaction 1. This was experimentally shown in Figures 1 and 3 and Figure S2, where both reactions Eq.1 and Eq.2 occurred simultaneously until complete inhibition of Eq.1 at the highest H_2O_2 amount (200 µM). Though H_2O_2 was full decomposed after 15 min of reaction time (Fig. S2), the suppressive effect on the birnessite reactivity was still observed over 24 h of reaction time (Fig. 1). This was confirmed by carrying out sequentially the reactions (Eq.2) and (Eq.1). Indeed, suppression of BPA removal capacity was also observed when MnO_2 and H_2O_2 were allowed to react first (*i.e.* pre-equilibration step of 30 min) until total decomposition of H_2O_2 before addition of BPA (Fig. S6). Therefore, the H_2O_2-mediated reduction of MnO_2 (Eq.2) considerably affects the surface reactivity of birnessite and its ability to remove BPA. This reductive dissolution generates Mn(II) ions which will in turn bind to MnO_2 surfaces and then be oxidized into higher valence Mn:

$$Mn^{II} + MnO_2 \rightarrow Mn^{II}/Mn^{III} - MnO_2 \qquad \text{(Eq.3)}$$

This oxidation reaction may be made possible by the residual H_2O_2 and/or generated O_2 (through Eq.2), which is pH-dependent. The contribution of O_2 from ambient air is excluded since reactivity assessment tests investigated under aerobic *vs* anaerobic conditions showed similar behavior in term of BPA removal.

It is worth noting that strong aggregation of MnO_2 particles and then fast sedimentation was

observed upon addition of H_2O_2. This phenomenon can be ascribed to charge neutralization (*i.e.* surface charge switch from negative to positive) upon Mn(II) ions binding to negatively charged MnO_2 surfaces, as previously reported.[55] Furthermore, disproportionation/comproportionation reaction (Eq.4) may occur within the MnO_2, *i.e.* Mn^{II} exchanges electrons with Mn(IV) to form two Mn(III) centers and, conversely, two Mn(III) centers can disproportionate to form Mn(II) and Mn(IV) centers[12,32,35,51,56]:

$$Mn^{II} + Mn^{IV} \leftrightarrow 2Mn^{III} \quad \text{(Eq.4)}$$

Since this reaction is pH-dependent, we have measured the average oxidation state (AOS) of birnessite over the whole investigated pH range (4-8). The AOS of samples reacted with BPA (25 μM) alone only slightly decreased from 3.98 to 3.90 (±0.02). However, partial reduction of MnO_2 upon addition of 200 μM of H_2O_2 dropped down the AOS to 3.74 (±0.04) at pH 4 and 6.5, and 3.61 (±0.04) at pH 8. This decrease suggests that percentages of Mn(III) or Mn(II) or both are relatively higher at the end of reaction with respect to the initial sample. The formation of Mn(III) was further confirmed by the detection of Mn(III)-pyrophosphate complex at 480 nm, Mn(III) being stabilized through ligand-binding complexes.[57]The effect of H_2O_2 on the structure of birnessite will be discussed in the following section.

Collectively, these results suggest that the H_2O_2 induced reduction of MnO_2 is an effective process, and the fast generation of Mn(II) is key for suppressed oxidative capacity of MnO_2 towards BPA. To confirm the impact of Mn(II) on the reactivity of MnO_2, BPA removal kinetics were investigated in Mn(II)-amended birnessite suspensions in the following section.

3.2. Effects of Mn(II) on the removal capacity of MnO_2

The initial rate constants of BPA removal sharply decreased with increasing in dissolved Mn(II) amount at pH 4 and 6.5, while at pH 8 it increased first between 0 and 10 μM but later decreased with increasing in initial Mn(II) amount (Fig. 5). It is previously reported that the

adsorption of cations such as Ca(II) or Mg(II) may change the surface charge from negative to positive by exchange of H^+ on the MnO_2 surface.[58,59] Similarly, the Mn(II) adsorption should lead to a decrease in the negative surface charge, thereby altering the binding capacity of MnO_2. When the Mn(II) amount further increases, we speculate a competition between BPA and Mn(II) to bind at reactive sites of MnO_2 during the first kinetic phase, as recently observed for quinolones.[43]

As for H_2O_2, dissolved Mn(II) displayed suppressive effects on the removal rate of BPA and the rate constants over the whole Mn(II) concentration range (10 - 100μM) exhibited the same order, pH 4 > pH 6.5 > pH 8 (Fig. 5). In addition to the comproportionation reaction that is pH-dependent, the decrease in the oxidative ability of MnO_2 in the presence of dissolved Mn(II) may result from competition of compound and Mn(II) to interact with reactive surface sites. The strong binding of Mn(II) to MnO_2 surfaces suggests competition of BPA and Mn(II) for surface sites, which is pH dependent.[33,45] Adsorption tests showed that 100 μM of Mn(II) were completely removed at both pH 6.5 and 8 (i.e. dissolved Mn(II) was below the detection limit), while 70 % of the added Mn(II) was removed at pH 4.

To check the affinity of birnessite for Mn(II) binding, sorption isotherms were determined at three pH values (4, 6.5 and 8) under aerobic conditions (Fig. S7). It should be noted that Mn(II) removal under oxic conditions is expected to be higher than under anoxic conditions, especially at alkaline pH values, which has been attributed to surface-catalyzed oxidation of Mn(II) by molecular oxygen.[49,50] Here, only aerobic conditions were tested, since the aim of these sorption isotherms is to assess the Mn(II) affinity under oxidizing conditions imposed by the presence of H_2O_2. As expected, Mn(II) binding to MnO_2 surfaces increased with pH increasing. Sorption isotherms showed different shape depending on pH value across the Mn(II) concentration range. At pH 4 a typical L-shape with a plateau was observed, while the removal amount continuously increased with Mn(II) concentration at higher pH values. This

high binding of Mn(II) at high pH value could cause Mn(III) enrichment in MnO_2 surfaces. [49,50]Some studies have shown that at high Mn(II)/Mn(IV) ratio and pH > 7.5, dissolved Mn(II) can interact with hexagonal birnessite and then transfer electron to lattice Mn(IV) producing Mn(III).[49,50] The buildup of Mn(III) will induce changes in mineral structure and composition by converting birnessite into lower-valence Mn phases. XRD analysis conducted on samples reacted with 100 μM of dissolved Mn(II) (Mn(II)/MnO_2 molar ratio = 0.3) showed no notable transformation of MnO_2 over the investigated pH range (Fig. 4). However, titration experiments showed that addition of 100 μM of dissolved Mn(II) dropped down the AOS of MnO_2 from 3.98 to 3.60 (±0.05) at pH 4 and 6.5, and 3.50 (±0.05) at pH 8, suggesting more Mn(III) or Mn(II) at the end of reaction with respect to the initial sample. A recent work showed that birnessite transformation into triclinic birnessite and/or 4 × 4 tunneled Mn oxide may occur at low Mn(II)/MnO_2 ratios (0.09 and 0.13), while secondary phases such as MnOOH and Mn_3O_4 can be generated at high Mn(II)/MnO_2 ratios (0.5 and 1). [60]In our XRD patterns, broad bands (hump) have appeared between 12° and 22° and between 25° and 35° in the samples reacted with Mn(II) (Mn(II)/MnO_2 molar ratio = 0.3) or H_2O_2 (H_2O_2/MnO_2 molar ratio = 0.6), suggesting changes in the structure or ordering of the birnessite mineral sheets (Fig. 4). We also observed these broad bands in the XRD pattern of synthetic Mn(III)-rich birnessite sample (see Fig. 4). This is consistent with previous studies, which suggested that Mn^{III} formation can be made in edge-sharing complexes on MnO_2 edge sites or around vacancy sites in octahedral layers of MnO_2.[5] In addition, a small peak near 20° only present in the patterns of samples reacted at pH 8 would suggest the presence of feitknechtite (β-MnOOH), as previously reported.[49]

3.3. Synergistic effects of anions and H_2O_2 on the oxidative activity of MnO_2

To check whether the suppression of reactivity at environmental relevant concentrations

of H_2O_2 can persist in presence of naturally occurring compounds, the initial rate constants k (h^{-1}) of BPA removal were determined at pH 6.5 in presence of silicate, nitrate and phosphate, commonly found in natural systems (Fig. 6). At 0 μM of H_2O_2, the presence of 100 μM of anions did not significantly influence the removal rate of BPA, probably because of weaker interactions of these anionic ligands with MnO_2 surfaces under the experimental conditions of this study (pH 6.5, 100 μM of anion, 345 μM of MnO_2). However, significant decrease in kinetic rate constants was observed in presence of silicate and phosphate when H_2O_2 was added in the reaction medium (H_2O_2/MnO_2 molar ratio between 0.03 and 0.3), while no impact on the reactivity was observed in presence of nitrate (Fig. 6). These results can be explained if the Mn(II) generated through H_2O_2-induced reduction of MnO_2 renders the MnO_2 surfaces more able to bind anionic ligands, thereby altering the surface reactivity towards BPA.

It was previously reported that unlike nitrate, silicate or phosphate may interact with MnO_2 through hydrogen bonding or formation of outer-sphere complexes with surface hydroxyl groups of MnO_2.[59-62] On the other hand, previous studies reported that the presence of dissolved silicate may decrease the oxidation rate constants of MnO_2 toward chlorinated compounds.[63,64] They have attributed the decrease in MnO_2 reactivity to the surface-bound silicate but none of them have provided adsorption data of silicate onto MnO_2. In the present work, we showed that silicate or phosphate has a very low affinity to the negatively charged MnO_2 surfaces under our experimental conditions, but the presence of 100 μM of Mn(II) significantly enhanced their adsorption amounts onto MnO_2 (Fig. S8). This increased adsorption might be due to the changes in both the surface charge of MnO_2 and the solution speciation of anionic ligands in the presence of divalent cations such as Mn(II). Indeed, the ligand speciation may be modified, since different coordination modes of aqueous complexes of phosphate with Mn(II) ions have been previously reported.[65] However, no precipitation is possible under our experimental conditions due to the low degree of saturation, resulting from

the very low aqueous concentration of ligand and complete removal of dissolved Mn(II) by adsorption (log K_s Mn(II)/phosphate = - 27.07).[66] Furthermore, Mn(II) binding should lead to a decrease in the negative surface charge, thereby enhancing ability to bind anions through electrostatic interactions.[55,58,59] Therefore, the MnO_2-bound Mn(II) system could adsorb more effectively anions such as phosphate or silicate through cation bridging, as recently reported for humic acid.[55] This surface-Mn(II)-ligand ternary complex may act as a barrier to electron transfer between BPA and Mn(IV) sites, thereby altering reactivity of MnO_2 surfaces.

It should be noted that the decomposition of H_2O_2 (200 μM) was found to be similar in presence or absence of silicate or phosphate (100 μM) (Fig. S9). Previous works have investigated the catalytic activity of manganese oxides for hydrogen peroxide decomposition and generation of reactive oxygen species in the context of environmental remediation studies.[29-31] Despite silicate adsorption on MnO_2 surfaces was found negligible, there was an inhibition effect on the H_2O_2 decomposition rate over the investigated silicate concentration range (0 to 1.5 mM). [30,67] Although these works have used different experimental conditions (*e.g.* much higher concentration of ligands or H_2O_2), and different MnO_2 types, the present findings call for in-depth consideration of the combined/synergistic effects that the cations and anions co-presents in the reaction medium may have on the MnO_2 reactivity. Overall, these findings suggest that Mn(II) generation through H_2O_2-mediated reduction may alter both adsorption and redox transformation of environmental compounds.

4. Conclusions

Photochemical and dark production of H_2O_2 make it ubiquitous not only in oceanic and atmospheric systems but also in the subsurface environment. Here, we have notably demonstrated that environmental levels of hydrogen peroxide can induce reductive dissolution of MnO_2 into Mn(II), thereby affecting the surface reactivity of MnO_2. As the H_2O_2

decomposition is a fast process, the generated dissolved Mn(II) binds to MnO_2 surfaces, altering further interactions with co-existing organic compounds. This may result from competition of organic compound and Mn(II) to interact with reactive surface sites and/or aqueous complexation with Mn(II). The presence of silicate or phosphate at concentrations comparable to those encountered in natural waters further decreased the reactivity of MnO_2 in presence of H_2O_2. Birnessite-bound Mn(II) adsorbed more effectively anionic ligands such as phosphate or silicate and thus reducing interactions with BPA at a range of environmentally relevant pH values. These findings suggest that naturally occurring anions and H_2O_2 may have synergetic effects on the reactivity of nanostructured birnessite-type manganese oxide. As manganese oxides can break down high molecular weight humic substances into lower molecular weight organic molecules and/or stabilize dissolved organic carbon, these findings call for in-depth consideration of the impacts of environmental levels of H_2O_2 and co-exiting anions on the global carbon cycle. Furthermore, the widespread presence of H_2O_2 in surface and ground water systems and associated impacts on the redox-active minerals should be considered in contaminant fate and transport assessment.

Conflicts of interest

There are no conflicts to declare.

Acknowledgments

This work was supported by the Institut Universitaire de France, the Region Council of Auvergne Rhône-Alpes and the CNRS. We gratefully acknowledge the Chinese Scholarship Council of PR China for providing financial support for Daqing Jia and Qinzhi Li.

Supplementary Material

Additional information regarding synthesis and characterization methods, SEM/TEM images, additional data on BPA removal kinetics, fitting procedures and H_2O_2 decomposition rate, silicate and phosphate speciation and their adsorption data onto MnO_2.

Reference

1 J. E. Post, Manganese oxide minerals: Crystal structures and economic and environmental significance, *Proc. Natl. Acad. Sci.*, 1999, **96**, 3447-3454.

2 Y. Wang, S. Benkaddour, F. F. Marafatto and J. Peña, Diffusion-and pH-dependent reactivity of layer-type MnO_2: Reactions at particle edges versus vacancy sites, *Environ. Sci. Technol.*, 2018, **52**, 3476-3485.

3 N. Birkner and A. Navrotsky, Thermodynamics of manganese oxides: Sodium, potassium, and calcium birnessite and cryptomelane, *Proc. Natl. Acad. Sci. U.S.A.*, 2017, **114**, E1046-E1053.

4 S. Wick, J. Peña and A. Voegelin, Thallium sorption onto manganese oxides, *Environ. Sci. Technol.*, 2019, **53**, 13168–13178.

5 B. J. Lafferty, M. Ginder-Vogel, M. Zhu, K. J. Livi and D. L. Sparks, Arsenite oxidation by a poorly crystalline manganese-oxide. 2. Results from X-ray absorption spectroscopy and X-ray diffraction, *Environ. Sci. Technol.*, 2010, **44**, 8467-8472.

6 C. K. Remucal and M. Ginder-Vogel, A critical review of the reactivity of manganese oxides with organic contaminants, *Environ. Sci. Process. Impacts.*, 2014, **16**, 1247−1266.

7 R. Pokharel, Q. Li, L. Zhou and K. Hanna, Water flow and dissolved Mn(II) alter transformation of pipemidic acid by manganese oxide, *Environ. Sci. Technol.*, 2020, **54**, 8051-8060.

8 J. Huang and H. Zhang, Redox reactions of iron and manganese oxides in complex systems, *Front. Environ. Sci. Eng.*, 2020, **14,** 76.

9 A. N. Ricko, A. W. Psoras and J. D. Sivey, Reductive transformations of dichloroacetamide safeners: effects of agrochemical co-formulants and iron oxide manganese oxide binary-mineral systems, *Environ. Sci.: Processes Impacts.*, 2020, **22,** 2104-2116.

10 M. Villalobos, B. Lanson, A. Manceau, B. Toner and G. Sposito, Structural model for the biogenic Mn oxide produced by Pseudomonas putida, *Am. Mineral.*, 2006, **91,** 489-502.

11 S. M. Webb, B. M. Tebo and J. R. Bargar, Structural characterization of biogenic Mn oxides produced in seawater by the marine bacillus sp. strain SG-1, *Am. Mineral.*, 2005, **90,** 1342-1357.

12 M. Zhu, M. Ginder-Vogel, S. J. Parikh, X.-H. Feng and D. L. Sparks, Cation effects on the layer structure of biogenic Mn-oxides, *Environ. Sci. Technol.*, 2010, **44,** 4465-4471.

13 M. Villalobos, B. Toner, J. Bargar and G. Sposito, Characterization of the manganese oxide produced by Pseudomonas putida strain MnB1, *Geochim. Cosmochim. Acta.*, 2003, **67,** 2649-2662.

14 W. J. Cooper and D. R. Lean, Hydrogen peroxide concentration in a northern lake: Photochemical formation and diel variability, *Environ. Sci. Technol.*, 1989, **23,** 1425–1428.

15 R. G. Zika, J. W. Moffett, R. G. Petasne, W. J. Cooper and E. S. Saltzman, Spatial and temporal variations of hydrogen peroxide in gulf of Mexico waters, *Geochim. Cosmochim. Acta.*, 1985, **49,** 1173–1184.

16 B. Gonzalez-Flecha and B. Demple, Homeostatic regulation of intracellular hydrogen peroxide concentration in aerobically growing, *Escherichia Coli. J. Bacteriol.*, 1997, **179,** 382–388.

17 F. Guillén, A. T. Martinez and M. J. Martínez, Production of hydrogen peroxide by aryl-alcohol oxidase from the ligninolytic fungus Pleurotus Eryngii, *Appl. Microbiol. Biotechnol.*, 1990, **32,** 465–469.

18 S. Garg, A. L. Rose and T. D. Waite, Photochemical Production of Superoxide and Hydrogen Peroxide from Natural Organic Matter, *Geochim. Cosmochim. Acta.*, 2011, **75,** 4310–4320.

19 J. W. Moffett and O. C. Zajiriou, An investigation of hydrogen peroxide chemistry in surface waters of vineyard sound with H218O2 and 18O2, *Limnol. Oceanogr.*, 1990, **35,** 1221–1229.

20 K. L. Roe, R. J. Schneider, C. M. Hansel and B. M. Voelker, Measurement of dark, particle-generated superoxide and hydrogen peroxide production and decay in the subtropical and temperate North Pacific Ocean, *Deep Sea Res. Part I Oceanogr. Res. Pap.*, 2016, **107,** 59–69.

21 W. J. Cooper, J. K. Moegling, R. J. Kieber and J. J. Kiddle, A chemiluminescence method for the analysis of H2O2 in natural waters, *Mar. Chem.*, 2000, **70,** 191–200.

22 X. Yuan, P. S. Nico, X. Huang, T. Liu, C. Ulrich, K. H. Williams and J. A. Davis, Production of hydrogen peroxide in groundwater at rifle, Colorado, *Environ. Sci. Technol.*, 2017, **51,** 7881–7891.

23 P. Liao, K. Yu, Y. Lu, P. Wang, Y. Liang and Z. Shi, Extensive dark production of hydroxyl radicals from oxygenation of polluted river sediments, *Chem. Eng. J.*, 2019, **368,** 700–709.

24 E. Kim, Y. Liu, C. J. Baker, R. Owens, S. Xiao, W. E. Bentley and G. F. Payne, Redox-cycling and H2O2 generation by fabricated catecholic films in the absence of enzymes, *Biomacromolecules.,* 2011, **12,** 880–888.

25 S. E. Page, G. W. Kling, M. Sander, K. H. Harrold, J. R. Logan, K. McNeill and R. M. Cory, Dark Formation of hydroxyl radical in arctic soil and surface waters, *Environ. Sci. Technol.,* 2013, **47,** 12860–12867.

26 J. D. Begg, M. Zavarin and A. B. Kersting, Plutonium desorption from mineral surfaces at environmental concentrations of hydrogen peroxide, *Environ. Sci. Technol.,* 2014, **48,** 6201-6210.

27 H.-P. Li, C. M. Yeager, R. Brinkmeyer, S. Zhang, Y.-F. Ho, C. Xu, W. L. Jones, K. A. Schwehr, S. Otosaka and K. A. Roberts, Bacterial production of organic acids enhances H2O2-dependent iodide oxidation, *Environ. Sci. Technol.,* 2012, **46,** 4837–4844.

28 M. Amme, W. Bors, C. Michel, K. Stettmaier, G. Rasmussen and M. Betti, Effects of Fe(II) and hydrogen peroxide interaction upon dissolving UO2 under geologic repository conditions, *Environ. Sci. Technol.,* 2005, **39,** 221−229.

29 R. J. Watts, J. Sarasa, F. J. Loge and A. L. Teel, Oxidative and reductive pathways in manganese-catalyzed Fenton's reactions, *J. Environ. Eng.,* 2005, **131,** 158-164.

30 A. L.-T. Pham, F. M. Doyle and D. L. Sedlak, Inhibitory effect of dissolved silica on H_2O_2 decomposition by iron(III) and manganese(IV) oxides: Implications for H_2O_2-based in situ chemical oxidation, *Environ. Sci. Technol.,* 2012, **46,** 1055–1062.

31 M. Kamagate, M. Pasturel, M. Brigante and K. Hanna, Mineralization enhancement of pharmaceutical contaminants by radical-based oxidation promoted by oxide-bound metal ions, *Environ. Sci. Technol.,* 2019, 5**4,** 476-485.

32 S. Balgooyen, P. J. Alaimo, C. K. Remucal and M. Ginder-Vogel, Structural transformation of MnO2 during the oxidation of bisphenol A, *Environ. Sci. Technol.,* 2017, **51,** 6053-6062.

33 K. Lin, W. Liu and J. Gan, Oxidative removal of bisphenol A by manganese dioxide: efficacy, products, and pathways, *Environ. Sci. Technol.,* 2009, **43,** 3860-3864.

34 J. Huang, S. Zhong, Y. Dai, C.-C. Liu and H. Zhang, Effect of MnO2 phase structure on the oxidative reactivity toward bisphenol A degradation, *Environ. Sci. Technol.,* 2018, **52,** 11309–11318.

35 S. Balgooyen, G. Campagnola, C. K. Remucal and M. Ginder-Vogel, Impact of bisphenol A influent concentration and reaction time on MnO2 transformation in a stirred flow reactor, *Environ. Sci. Process. Impacts.,* 2019, **21,** 19–27.

36 R. M. McKenzie, The synthesis of birnessite, cryptomelane, and some other oxides and hydroxides of manganese, *Mineral. Mag.,* 1971, **38,** 493-502.

37 Q. Sun, P. X. Cui, T. T. Fan, S. Wu, M. Zhu, M. E. Alves, D. M. Zhou and Y. J. Wang, Effects of Fe (II) on Cd (II) immobilization by Mn (III)-rich δ-MnO2, *Chem. Eng. J.,* 2018, **353,** 167-175.

38 A. A. Simanova, K. D. Kwon, S. E. Bone, J. R. Bargar, K. Refson, G. Sposito and J. Peña, Probing the sorption reactivity of the edge surfaces in birnessite nanoparticles using nickel (II), *Geochim. Cosmochim. Acta.,* 2015, **164,** 191-204.

39 Y. Wu, M. Passananti, M. Brigante, W. Dong and G. Mailhot, Fe (III)–EDDS Complex in Fenton and photo-Fenton processes: From the radical formation to the degradation of a target compound, *Environ. Sci. Pollut. Res.,* 2014, **21,** 12154–12162.

40 T. Charbouillot, M. Brigante, G. Mailhot, P. R. Maddigapu, C. Minero and D. Vione, Performance and selectivity of the terephthalic acid probe for OH as a function of temperature, pH and composition of atmospherically relevant aqueous media, *J. Photochem. Photobiol. A.*, 2011, **222,** 70-76,

41 J. Mullin and J. Riley, The colorimetric determination of silicate with special reference to sea and natural waters, *Anal. Chim. Acta.,* 1955, **12,** 162-176.

42 V. Ruiz-Calero and M. T. Galceran, Ion chromatographic separations of phosphorus species: a review, *Talanta.,* 2005, **66,** 376-410.

43 Q. Li, R. Pokharel, L. Zhou, M. Pasturel and K. Hanna, Coupled effects of Mn(II), pH and anionic ligands on the reactivity of nanostructured birnessite, *Environ. Sci. Nano.,* 2020, **7,** 4022-4031.

44 J. Im, C. W. Prevatte, S. R. Campagna and F. E. Löffler, Identification of 4-hydroxycumyl alcohol as the Major MnO2-mediated bisphenol A transformation product and evaluation of its environmental fate, *Environ. Sci. Technol.*, 2015, **49,** 6214-6221.

45 H. Zhang, W. R. Chen and C. H. Huang, Kinetic modeling of oxidation of antibacterial agents by manganese oxide, *Environ. Sci. Technol.*, 2008, **42,** 5548-5554.

46 W. Stumm and J. J. Morgan, Aquatic chemistry: Chemical equilibria and rates in natural waters, John Wiley & Sons., 2012.

47 S. Baral, C. Lume-pereira, E. Janata and A. Henglein, Chemistry of colloidal manganese dioxide. Part 2. Reaction with O2-and H2O2 (Pulse radiolysis and stop flow studies), *J. Phys. Chem.*, 1985, **89,** 5779-5783.

48 D. B. Broughton and R. L.Wentworth, Mechanism of decomposition of hydrogen peroxide solutions with manganese dioxide. I, *J. Am. Chem. Soc.*, 1947, **69,** 741–744.

49 J. P. Lefkowitz, A. A. Rouff and E. J. Elzinga, Influence of pH on the reductive transformation of birnessite by aqueous Mn(II), *Environ. Sci. Technol.*, 2013, **47,** 10364-10371.

50 E. J. Elzinga, Reductive transformation of birnessite by aqueous Mn(II), *Environ. Sci. Technol.*, 2011, **45,** 6366-6372.

51 Q. Wang, P. Yang and M. Zhu. Structural Transformation of Birnessite by Fulvic Acid under Anoxic Conditions, *Environ. Sci. Technol.*, 2018, **52,** 1844–1853.

52 H. Yin, Y. Zhou, J. Xu, S. Ai, L. Cui and L. Zhu, Amperometric biosensor based on tyrosinase immobilized onto multiwalled carbon nanotubes-cobalt phthalocyanine-silk fibroin film and its application to determine bisphenol A, *Anal. Chim. Acta.*, 2010, **659,** 144-150.

53 H. Yin, Y. Zhou, L. Cui, X. Liu, S. Ai and L. Zhu, Electrochemical oxidation behavior of bisphenol A at surfactant/layered double hydroxide modified glassy carbon electrode and its determination, *J. Solid State Electrochem.*, 2011, **15,** 167-173.

54 Ş. U. Karabiberoğlu, Sensitive voltammetric determination of bisphenol A based on a glassy carbon electrode modified with copper oxide ‐ zinc oxide decorated on graphene oxide, *Electroanalysis.*, 2019, **31,** 91-102.

55 H. Chenga, T. Yang, J. Jiang, X. Lu, P. Wanga and J. Ma, Mn2+ effect on manganese oxides (MnOx) nanoparticles aggregation in solution: Chemical adsorption and cation bridging, *Environ. Pollut.*, 2020, **267,** 115561.

56 H. Zhao, M. Zhu, W. Li, E. J. Elzinga, M. Villalobos, F. Liu, J. Zhang, X. Feng and D. L. Sparks, Redox Reactions between Mn (II) and Hexagonal Birnessite Change its Layer Symmetry, *Environ. Sci. Technol.*, 2016, **50,** 1750-1758.

57 S. M. Webb, G. J. Dick, J. R. Bargar and B. M. Tebo, Evidence for the presence of Mn(III) intermediates in the bacterial oxidation of Mn(II), *Proc. Natl. Acad. Sci.*, 2005, **102,** 5558-5563.

58 T. Takamatsu, M. Kawashima and M. Koyama, The role of Mn(II)-rich hydrous manganese oxide in the accumulation of arsenic in lake sediments, *Water. Res.*, 1985, **19,** 1029-1032.

59 W. Yao and F. J. Millero, Adsorption of phosphate on manganese dioxide in seawater, *Environ. Sci. Technol.*, 1996, **30,** 536-541.

60 P. Yang, K. Wen, K. A. Beyer, W. Xu, Q. Wang, D. Ma, J.Wu and M. Zhu, Inhibition of Oxyanions on Redox-driven Transformation of Layered Manganese Oxides, *Environ. Sci. Technol.*, 2021, **55,** 3419-3429.

61 S. Mustafa, M. I. Zaman and S. Khan, pH effect on phosphate sorption by crystalline MnO2, *J. Colloid Interface Sci.*, 2006, **301,** 370-375.

62 L. S. Balistrieri and T. T. Chao, Adsorption of selenium by amorphous iron oxyhydroxide and manganese dioxide, *Geochim. Cosmochim. Acta.*, 1990, **54,** 739-751.

63 S. Taujale and H. Zhang, Impact of interactions between metal oxides to oxidative reactivity of manganese dioxide, *Environ. Sci. Technol.*, 2012, **46,** 2764-2771.

64 M. Yu, X. He, B. Xi, Y. Xiong, Z. Wang, D. Sheng, L. Zhu and X. Mao, Dissolved Silicate Enhances the Oxidation of Chlorophenols by Permanganate: Important Role of Silicate-Stabilized MnO2 Colloids, *Environ. Sci. Technol.*, 2020, **54,** 10279–10288.

65 C. K. Sharma, C. C. Chusuei, R. Clérac, T. Möller, K. R. Dunbar and A. Clearfield, Magnetic property studies of manganese−phosphate complexes, *Inorg. Chem.*, 2003, **42,** 8300-8308.

66 G. Friedl, B. Wehrli and A. Manceau, Solid phases in the cycling of manganese in eutrophic lakes: New insights from EXAFS spectroscopy, *Geochim. Cosmochim. Acta.*, 1997, **61,** 275-290.

67 K. Hanna, Comment on "Inhibitory effect of dissolved silica on H_2O_2 decomposition by iron (III) and manganese (IV) oxides: implications for H_2O_2–based in situ chemical oxidation", *Environ. Sci. Technol*., 2012, **46**, 3591-3592.

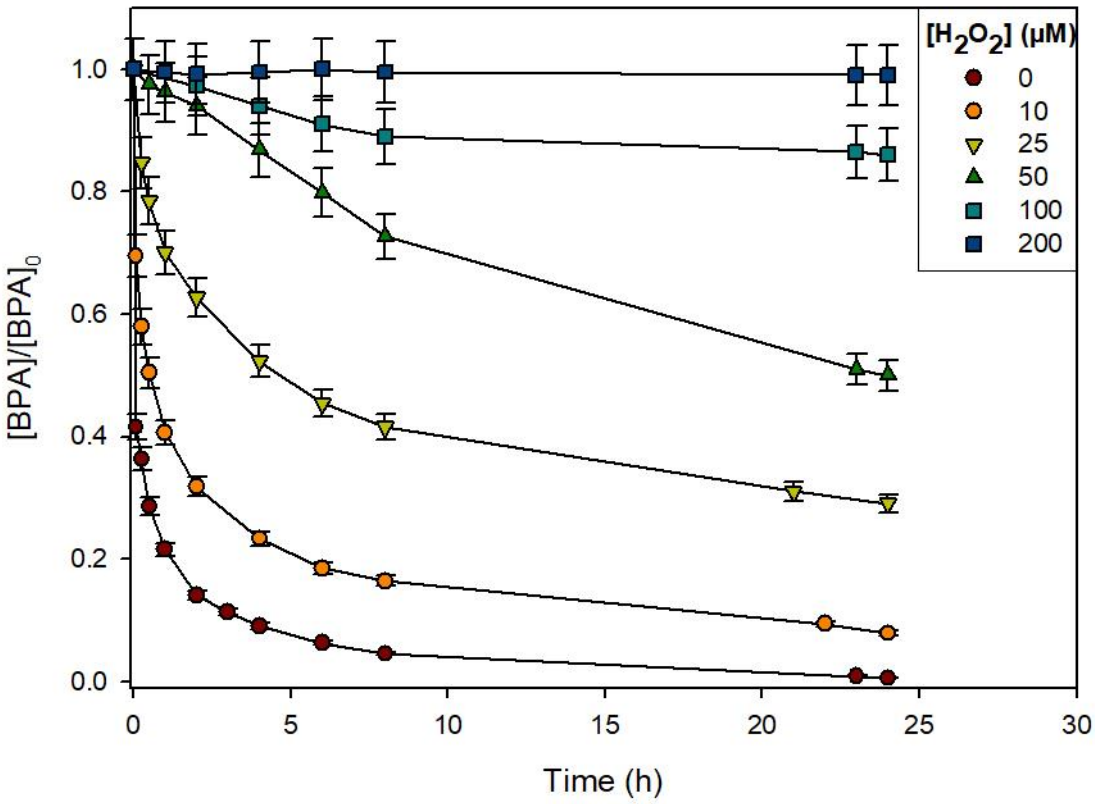

Figure 1. Effect of H_2O_2 concentration on the BPA removal at pH 6.5 at room temperature. Experimental conditions: [AB] = 345 μM, [BPA] = 25 μM. H_2O_2/MnO_2 ratio = 0 - 0.6. The relative experimental error lied at 5 % for BPA.

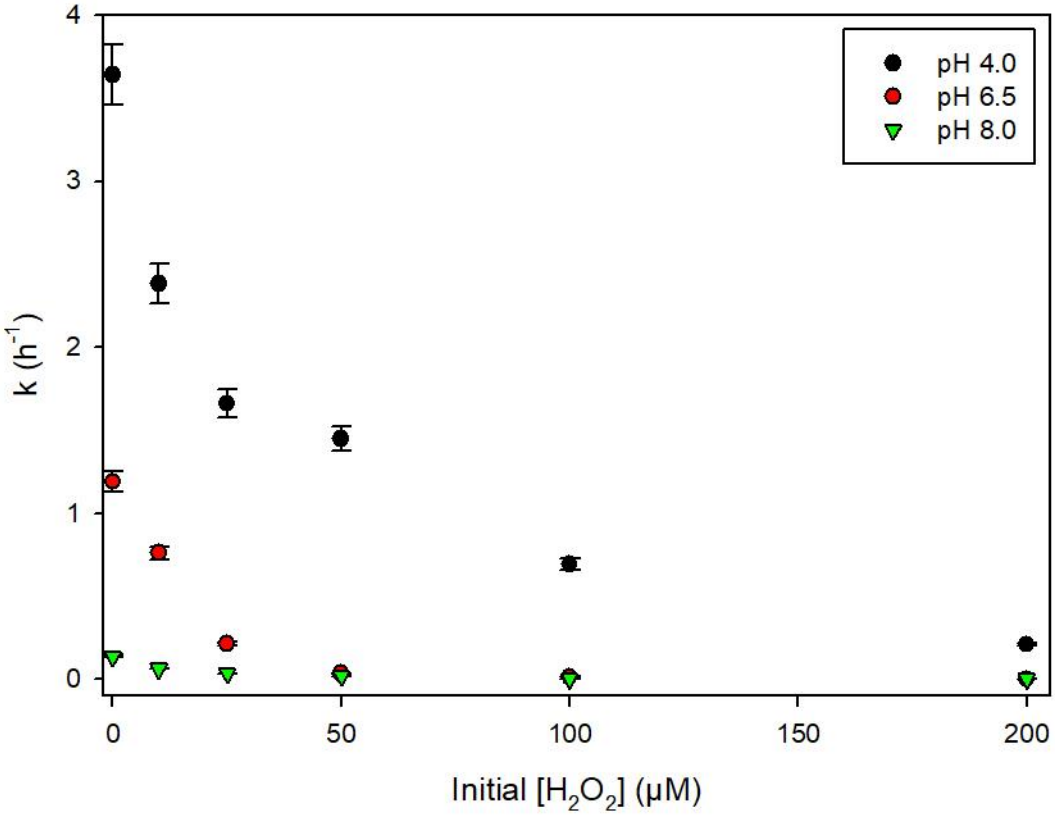

Figure 2. Removal rate constants (h^{-1}) of BPA as a function of H_2O_2 dose at three pH values (4, 6.5 and 8). Experimental conditions: [AB] = 345 µM, [BPA] = 25 µM, [H_2O_2] = 0 - 200 µM. H_2O_2/MnO_2 ratio = 0 - 0.6, room temperature. The relative experimental error lied at 5 %.

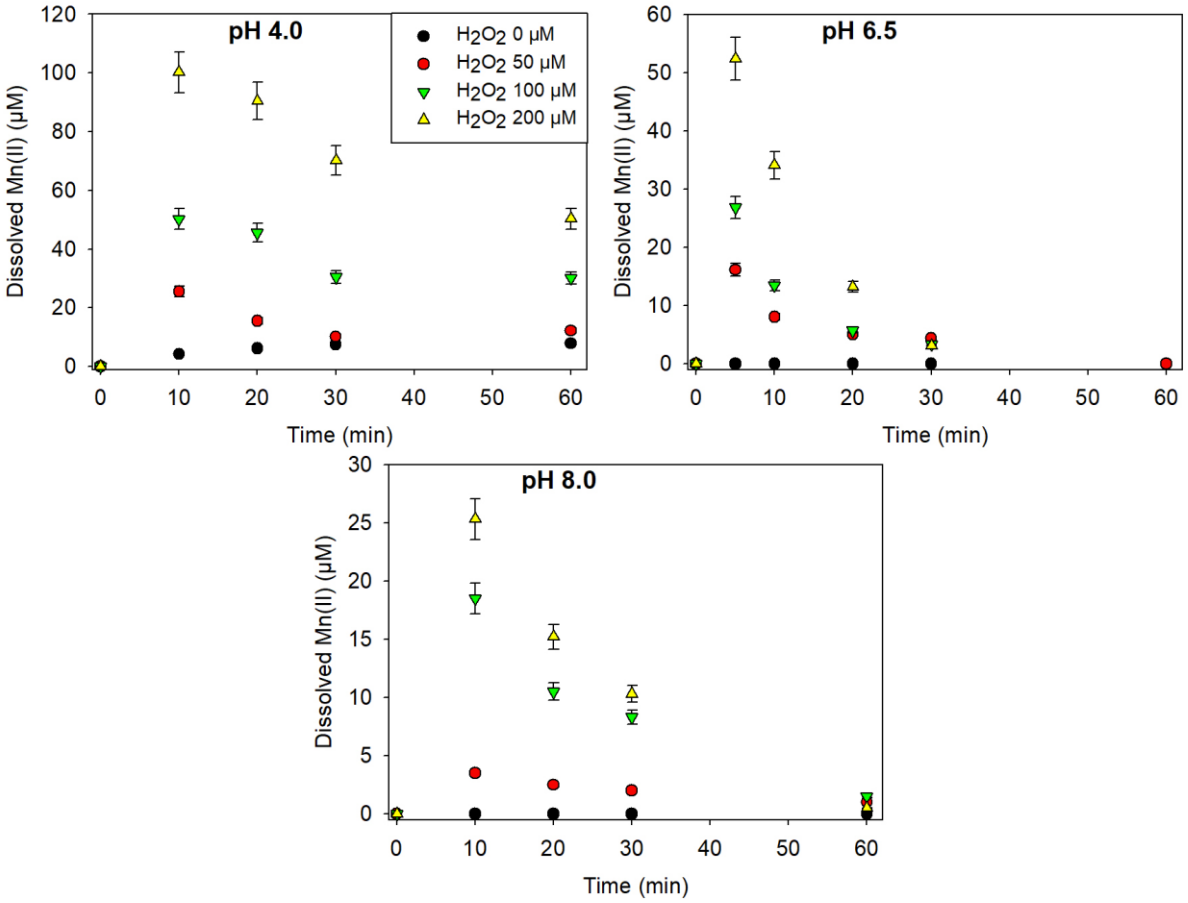

Figure 3. Mn(II) formation under different H_2O_2 concentrations and pH 4.0, 6.5 and 8.0. Experimental conditions: [AB] = 345 µM and [BPA] = 25 µM. H_2O_2/MnO_2 ratio = 0 - 0.6, room temperature. The relative experimental error lied at 7 % for Mn(II).

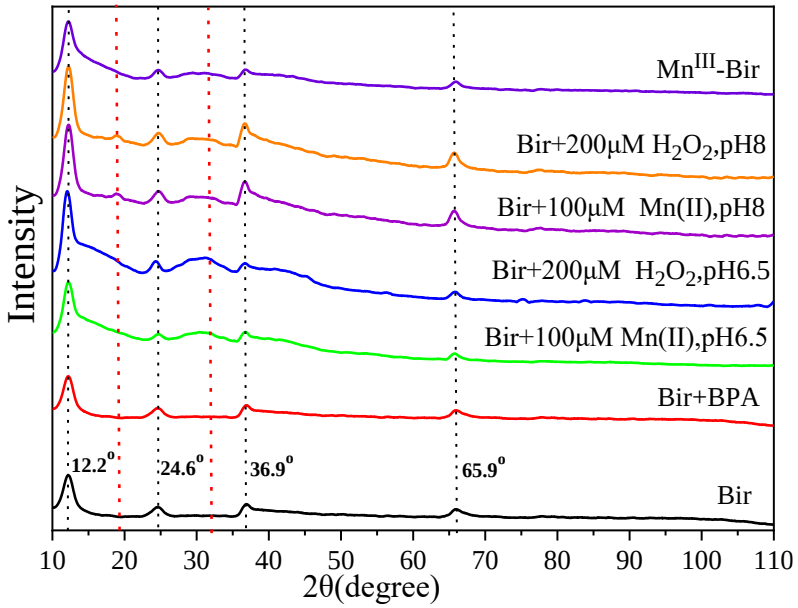

Figure 4. XRD patterns of birnessite before and after reaction in the presence of H_2O_2 or Mn(II) (two pH values, 24 h of reaction time), and of Mn(III) rich Birnessite. The black dashed lines indicate the peaks of acid birnessite, while the red dashed lines indicate broad bands appeared in reacted samples. Experimental conditions: [AB] = 345 μM and [BPA] = 25 μM. H_2O_2/MnO_2 ratio = 0.6. Mn(II)/MnO_2 ratio = 0.3. The solid was characterized using X-ray powder diffraction (XRD) with a Bruker AXS D8 Advance diffractometer (θ−2θ Bragg−Brentano geometry) using monochromated Cu $K\alpha_1$ (1.54Å) radiation.

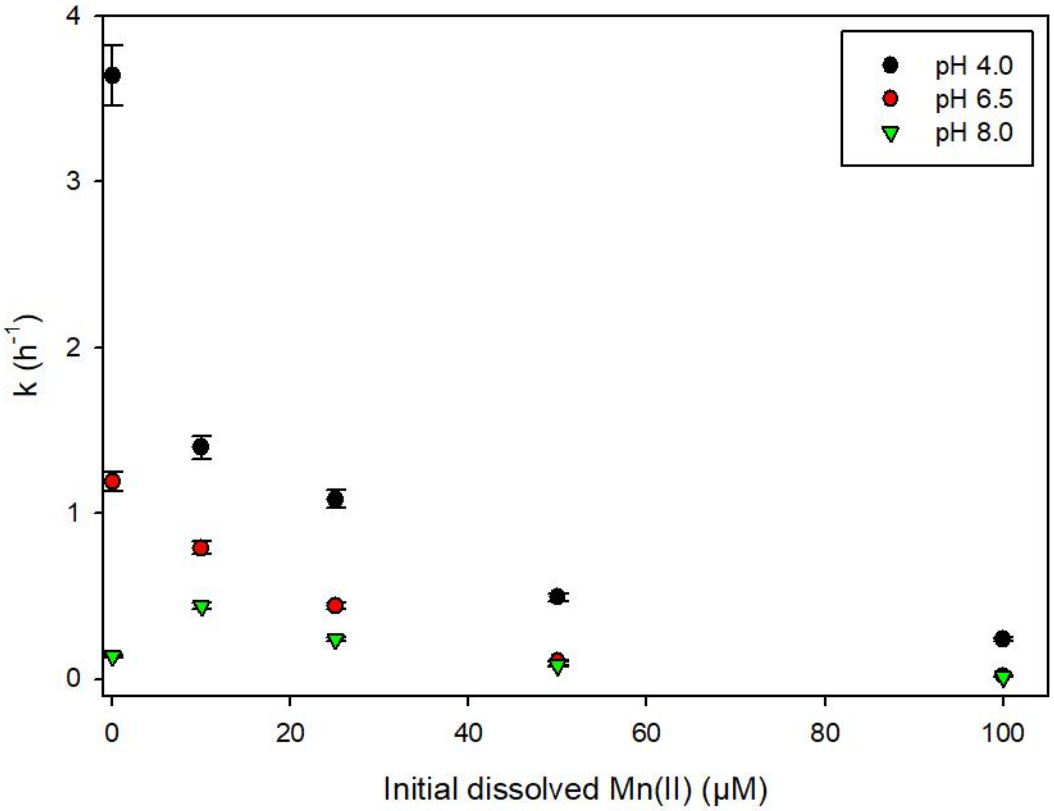

Figure 5. Removal rate constants (h^{-1}) of BPA as a function of Mn(II) concentration at three pH values (4, 6.5 and 8). Experimental conditions: [AB] = 345 µM, [BPA] = 25 µM, [Mn(II)] = 0 - 100 µM, room temperature. The relative experimental error lied at 5 %.

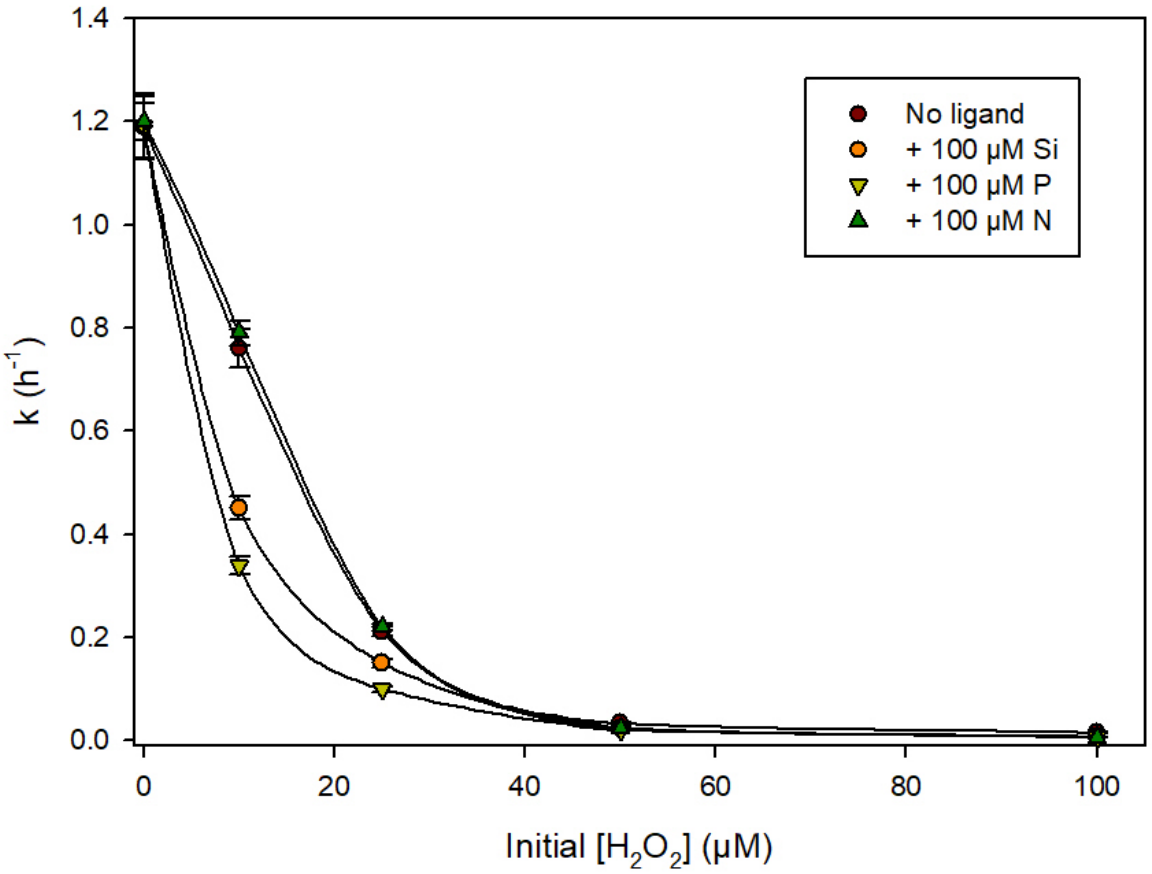

Figure 6. Removal rate constants (h^{-1}) of BPA as a function of H_2O_2 dose in absence or presence of silicate (Si), nitrate (N) or phosphate (P): Experimental conditions: pH 6.5, [AB] = 345 µM, [BPA] = 25 µM.; [Na_2SiO_3] = 100 µM; [$NaNO_3$] = 100 µM; [NaH_2PO_4] = 100 µM. H_2O_2/MnO_2 ratio = 0 - 0.3, room temperature. The relative experimental error lied at 5 %.